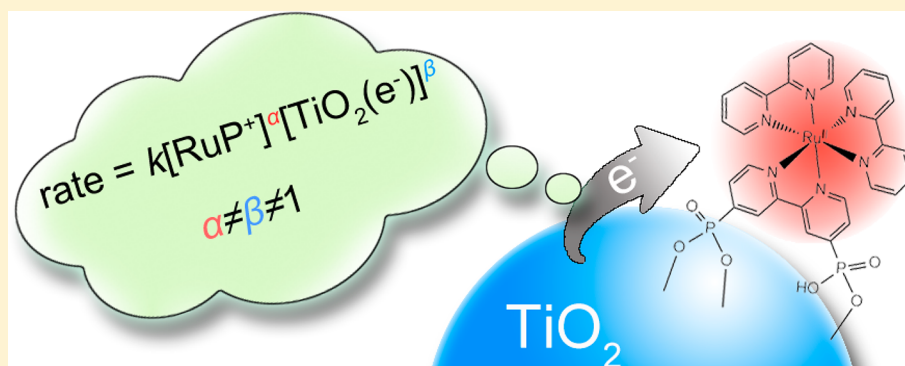


Charge Recombination with Fractional Reaction Orders in Water-Splitting Dye-Sensitized Photoelectrochemical Cells

Pengtao Xu,¹ Christopher L. Gray, Langqiu Xiao, and Thomas E. Mallouk*¹

Departments of Chemistry, Physics, and Biochemistry and Molecular Biology, The Pennsylvania State University, University Park, Pennsylvania 16802, United States

S Supporting Information

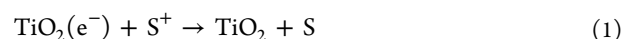


ABSTRACT: In water-splitting dye-sensitized photoelectrochemical cells (WS-DSPECs), charge recombination competes with catalytic water oxidation to determine the overall efficiency of the system. The kinetics of these processes have been difficult to understand because transient absorbance (TA) experiments typically show nearly complete charge recombination on the submillisecond time scale; in contrast, electrochemical measurements such as open circuit photovoltage decay suggest a charge recombination time scale that is 2–3 orders of magnitude longer. Here we explore these processes with dye-sensitized nanocrystalline TiO₂ and TiO₂/Ta₂O₅ core–shell photoanodes in aqueous electrolytes using TA spectroscopy, intensity-modulated photovoltage spectroscopy (IMVS), and photoelectrochemical impedance spectroscopy (PEIS). The fast recombination rates measured by TA result from strong laser excitation that leads to high electron occupancy in TiO₂, whereas IMVS modulates the concentration of charge-separated states near solar irradiance levels. The recombination processes measured by electrochemical methods such as IMVS, PEIS, and transient photovoltage are the discharging of injected electrons in TiO₂, as evidenced by the close agreement between the nearly first-order recombination rates probed by IMVS and the RC time constants derived from PEIS data. However, IMVS measurements at variable probe light intensity reveal that the reaction orders for the recombination of injected electrons with oxidized sensitizer molecules are far from unity. This kinetic analysis is relevant to understanding steady-state recombination rates in full WS-DSPECs in which molecular and nanoparticle catalysts are used to oxidize water.

INTRODUCTION

Water-splitting dye-sensitized photoelectrochemical cells (WS-DSPECs) represent a molecular approach to artificial photosynthesis.^{1–3} In these cells, photoexcited sensitizer molecules inject electrons into a semiconductor (typically mesoporous TiO₂ or a core–shell oxide semiconductor) and are regenerated by accepting electrons from a water oxidation catalyst. Because of the sluggish kinetics of the four-electron oxidation of water, recombination of the injected electrons with the oxidized sensitizer molecules is an important parasitic process in WS-DSPECs.^{4–6} Understanding the kinetics of forward and back electron transfer at the semiconductor–sensitizer interface is therefore important from both fundamental and device efficiency perspectives.

The recombination reaction that takes place at the semiconductor–sensitizer interface can be represented as follows:



where TiO₂(e[−]) and S⁺ represent the injected electrons in TiO₂ and the oxidized form of the sensitizer, respectively. The corresponding reaction rate law can be expressed for the bimolecular process as

$$\text{rate} = k[\text{S}^+]^\alpha [\text{TiO}_2(e^-)]^\beta \quad (2)$$

where *k* is the recombination rate coefficient, and the reaction orders of TiO₂(e[−]) and S⁺ are β and α, respectively. Under

Received: May 9, 2018

Published: August 27, 2018

photostationary open-circuit conditions, $\text{TiO}_2(\text{e}^-)$ and S^+ are present in equimolar amounts, and given the homogeneous structure of the porous sensitized electrode, these amounts are often expressed as local concentrations as in eq 2. Note that this model does not consider the lateral charge transfer between sensitizer molecules, because the hole-hopping time is on the orders of nanoseconds and therefore fast on the time scale of charge recombination.⁷

Early studies of this reaction used time-resolved transient absorption spectroscopy (TA) to monitor the bleaching recovery of S^+ species.^{8–10} It was found that there were slow and fast recombination events from the bleaching recovery signals, and they could be adequately fitted to the sum of two second-order equal-concentration processes, suggesting both α and β to be 1.¹⁰ However, Haque et al. showed that the recombination rate was strongly bias dependent.¹¹ A 600 mV shift in the TiO_2 conduction band could result in a 10^7 variation in recombination rate. This highly nonlinear dependence of the recombination rate precludes a second-order kinetic process.¹¹ Recently, by deliberately controlling the concentrations of $\text{TiO}_2(\text{e}^-)$ and S^+ through external bias, Brigham et al.¹² quantified both α and β to be 1 using the Ostwald isolation method. This method requires one of the species, either $\text{TiO}_2(\text{e}^-)$ or S^+ , to be in 10-fold excess in concentration, which allows the concentration of the other species to determine the recombination rate in pseudo first-order fashion. The conditions under which one species dominates the recombination reaction, however, strongly deviates from the actual operating conditions in which equal amounts of $\text{TiO}_2(\text{e}^-)$ and S^+ are present. The charging/discharging currents under external bias should shift the Fermi energy inside the TiO_2 away from the level that injected electrons would occupy, and this can potentially change the recombination mechanism relative to open-circuit conditions where $[\text{TiO}_2(\text{e}^-)]$ equals $[\text{S}^+]$. Therefore, results from the Ostwald isolation method may not be accurate for describing eq 2 under conditions relevant to photoelectrochemical water splitting.

In this work, we use intensity-modulated photovoltage spectroscopy (IMVS) to characterize eq 2 by monitoring the $\text{TiO}_2(\text{e}^-)$ concentration through the measured potential. Pioneered by Peter et al.,¹³ IMVS is a light-perturbation technique that is widely used to study charge recombination in photovoltaics and photoelectrochemical electrodes.^{14–17} In a typical measurement, a small sinusoidal modulation of light intensity is superimposed on the steady-state illumination of the photoelectrode and the modulation of photovoltage is measured simultaneously. The experiment can be conducted under open-circuit conditions without any external bias and at steady-state illumination intensities close to those of the operating water-splitting device. The TiO_2 Fermi level and filling of trap states are controlled solely by the injected electrons, allowing the recombination process to be studied under quasi-photostationary conditions.

We apply IMVS to study the charge recombination process in dye-sensitized photoelectrodes that have undergone different surface processing steps to improve their efficiency. Most reported electrodes for WS-DSPECs are sensitized with dye molecules immediately after the preparation of the mesoporous TiO_2 films (pristine electrodes). However, research on dye-sensitized solar cells has highlighted the importance of a TiCl_4 treatment on the TiO_2 films before dye sensitization, because this process can improve the solar cell efficiency.^{18,19} It

begins experimentally by soaking the electrodes coated with a mesoporous TiO_2 thin film into an aqueous TiCl_4 solution at 70 °C and then calcining the electrodes at 500 °C. This treatment is reported to deposit a thin TiO_2 shell on the mesoporous particles, passivating surface trap states, and improving the necking between particles, increasing the electron diffusion coefficient.¹⁸ It has also recently been applied to perovskite solar cells for improved performance.^{20–22} We also prepare a $\text{TiO}_2/\text{TaO}_x$ core-shell structure using atomic layer deposition (ALD). Coating a more insulating material over the mesoporous support can increase the energy barrier for back electron transfer of the injected electron through eq 1, extending the charge-separation lifetime, as evidenced from many spectroscopic and photoelectrochemical experiments.^{23–25}

Our results suggest that the molecularity of eq 1 is far from second-order and strongly depends on surface treatments. Unmodified electrodes exhibit a more unimolecular recombination process, whereas TiCl_4 -treated and $\text{TiO}_2/\text{TaO}_x$ electrodes show a recombination process that appears bimolecular. In all cases, however, α and β are not unity as previous reports suggest. Importantly, we observe a 3 orders of magnitude difference in the recombination lifetimes as measured by IMVS and TA. Comparing the injected electron concentrations, we conclude that faster recombination detected by TA stems from intense laser excitation, which results in high concentrations of charge-separated states that are inaccessible by injection at solar fluence. We also find from photoelectrochemical impedance spectroscopy that a simple RC time constant correlates well with the electron recombination lifetime.

THEORY

Open-Circuit Potential, Light Intensity, and Electron Recombination Rate. Adapting the analysis of charge recombination in the dye-sensitized solar cell given by Huang et al.,²⁶ we can express the recombination current density in a dye-sensitized photoanode as a bimolecular recombination process according to eq 3:

$$j_{\text{rec}} = qk_{\text{r}}c_{\text{RuP}}^{\alpha}(n - n_{\text{d}})^{\beta} \quad (3)$$

where k_{r} , c_{RuP} , and n_{d} are the recombination rate coefficient, the oxidized sensitizer concentration, and the TiO_2 electron concentration in the dark, respectively. The reaction order is expressed as α for oxidized sensitizer molecules and as β for electrons. The electron population in TiO_2 due to light-induced electron injection from sensitizer molecules follows:

$$n = n_{\text{d}} e^{q\Delta V/mkT} \quad (4)$$

where kT is the thermal energy and m is the ideality factor which is unity for an ideal diode.^{27,28} ΔV is the photoanode potential difference between dark (V_{dark}) and light (V_{light}) conditions:

$$\Delta V = V_{\text{dark}} - V_{\text{light}} \quad (5)$$

Note that because our electrodes were measured in a three-electrode configuration, V_{light} (the potential of the photoanode relative to a reference electrode) is more cathodic than V_{dark} . Substituting eq 5 into eq 4 and taking the derivative of V_{light} with respect to $\log n$, we obtain

$$\frac{dV_{\text{light}}}{d \log n} = -2.3mkT/q \quad (6)$$

In the absence of electron donors and under open-circuit conditions, the only route by which excited sensitizer molecules can be oxidized is by injecting electrons into TiO_2 . Therefore, the concentrations of the oxidized sensitizer and injected electrons are equal:

$$c_{\text{RuP}} = n - n_{\text{d}} \quad (7)$$

Comparing eqs S2 and 3, we can express the recombination rate (k_{IMVS}) measured by IMVS as

$$k_{\text{IMVS}} = k_{\text{r}} c_{\text{RuP}}^{\alpha} \quad (8)$$

From eqs S1, S3, and 3–7, we can formulate the relationship between V_{light} and light intensity (I_0) at steady-state and open-circuit conditions ($dn/dt = 0$, $j_{\text{ext}} = 0$) as follows:

$$AI_0 = k_{\text{r}} [n_{\text{d}} (e^{q\Delta V/mkT} - 1)]^{\alpha+\beta} \quad (9)$$

In a typical experiment, m is between 1 and 2, and ΔV is larger than 200 mV. Thus, $e^{q\Delta V/mkT} - 1 \approx e^{q\Delta V/mkT}$. Equation 9 can then be simplified to obtain the light intensity dependence of V_{light} according to the following expression:

$$V_{\text{light}} = V_{\text{dark}} - \frac{2.3mkT}{q(\alpha + \beta)} \log \frac{AI_0}{k_{\text{r}} n_{\text{d}}^{\alpha+\beta}} \quad (10)$$

In a plot of V_{light} as a function of $\log I_0$, the slope is therefore

$$\frac{dV_{\text{light}}}{d \log I_0} = -\frac{2.3mkT}{q(\alpha + \beta)} \quad (11)$$

Similarly, from eqs 4–8, we can express the potential dependence of k_{IMVS} as

$$V_{\text{light}} = V_{\text{dark}} - \frac{2.3mkT}{q\alpha} \log \frac{k_{\text{IMVS}}}{k_{\text{r}} n_{\text{d}}^{\alpha}} \quad (12)$$

The slope of $\log k_{\text{IMVS}}$ against V_{light} is

$$\frac{d \log k_{\text{IMVS}}}{dV_{\text{light}}} = -\frac{q}{2.3mkT} \quad (13)$$

■ EXPERIMENTAL SECTION

Photoanode Preparation. A colloidal TiO_2 nanoparticle paste was prepared by a previously reported method.²⁹ The paste was doctor-bladed onto a clean FTO substrate ($3 \times 5 \text{ cm}^2$, fluorine-doped SnO_2 -coated glass, $8 \Omega/\text{cm}^2$, Hartford Glass), followed by a sintering process at $300 \text{ }^\circ\text{C}$ for 20 min, $350 \text{ }^\circ\text{C}$ for 10 min, and $500 \text{ }^\circ\text{C}$ for 30 min. After cooling to room temperature, the FTO substrate was cut into five electrodes ($3 \times 1 \text{ cm}^2$). The thickness of the mesoporous TiO_2 film was measured by scanning electron microscopy to be about $3 \mu\text{m}$. TiCl_4 -treated samples were prepared by immersing the electrodes into a 50 mM aqueous TiCl_4 solution for 40 min at $70 \text{ }^\circ\text{C}$ before calcination at $500 \text{ }^\circ\text{C}$ for 30 min. Core-shell samples were prepared by depositing tantalum oxide over the TiCl_4 -treated films at $150 \text{ }^\circ\text{C}$ using atomic layer deposition (ALD, Cambridge Savannah 200). Pentakis(dimethylamino) tantalum(V) (heated at $90 \text{ }^\circ\text{C}$, > 98%, Strem Chemicals) was used as the tantalum source, and water vapor (ambient temperature) was the oxygen source. TaO_x films were formed by alternately pulsing each precursor (0.25 s for Ta, 0.015 s for water) into the sample chamber under a N_2 carrier gas flowing at 20 sccm. Due to the large surface area of the mesoporous TiO_2 film, we allowed a 60 s exposure time for each precursor to interact with the sample before it was purged by N_2 . A silicon wafer was placed inside the sample chamber during the deposition to monitor the growth of the TaO_x film. We performed four cycles of ALD for the TiO_2 electrode, and the deposited TaO_x film was 0.57 nm thick according to ellipsometry measurements. The as-prepared electrodes

were stored in a $70 \text{ }^\circ\text{C}$ oven before being soaked in a 0.1 mM ethanolic solution of bis(2,2'-bipyridine)(4,4'-diphosphonato-2,2'-bipyridine)ruthenium(II) bromide (RuP) for 20 h. The molecular sensitizer was prepared according to previous literature reports.³⁰ Following dye sensitization, the electrodes were rinsed with ethanol and dried in a compressed air stream before being stored in the dark for future use.

Photoelectrochemical Measurements. All photoelectrochemical measurements were carried out at ambient temperature ($23\text{--}24 \text{ }^\circ\text{C}$) in the three-electrode configuration using Ag/AgCl (3 M NaCl) as the reference electrode and Pt wire as the counter electrode. All potentials reported here are referenced to the reference electrode unless otherwise noted. The electrolyte was 10 mM acetic acid/sodium acetate solution (pH 4.7, degassed by purging with Ar). Intensity-modulated photovoltage spectroscopy (IMVS) was conducted using an Autolab potentiostat (PGSTAT128N) in combination with an Autolab LED Driver. A 470 nm LED light (LDC470, Metrohm), driven by the LED Driver, was used as the light source. The light intensity was controlled by changing the DC level of the LED current, and the light perturbation amplitude was set to be 10% of the DC level with a modulation frequency range between 400 and 1 Hz. IMVS measurements were carried out under open-circuit conditions (output current set to 0). Light intensity was measured by a Si photodiode (Thorlabs, S130C). Electrochemical impedance spectroscopy (EIS) was performed in galvanostatic mode under open-circuit conditions with 470 nm illumination. The applied frequency range was from 1000 to 1 Hz. The current perturbation was set to $5 \mu\text{A}$.

Nanosecond Transient Absorption Spectroscopy. A Q-switched Nd:YAG laser (Spectra Physics GCR-130) pulsed at 10 Hz provided the excitation beam (10 ns, 532 nm). The laser pulse energy (6.5 mJ) was measured by using a pyroelectric energy sensor (ES220C, Thorlabs). A 470 nm LED coupled into an optical fiber was used to provide the probe light. The probe beam, oriented perpendicular to the laser beam, was continuously on in each measurement (100 laser shots). A monochromator (Spectral Products CM110) was placed in front of the detector, a gated photomultiplier tube (Hamamatsu H10304-01-NF). Two notch filters (532 nm) were also placed before the detector to minimize scattered light from the laser. The signal was recorded using an oscilloscope (PicoScope 6404c) that was optically triggered by a Si photodiode (Thorlabs DET36A). The laser pulse and PMT gate timing were controlled by a pulse generator (Berkeley Nucleonics Corporation, model 505). The response time of the whole system was about 30 ns.

The sample was positioned at a 45° angle to both the laser beam and the probe beam. We noticed that the PMT output signals became saturated under intense probe light, showing a nonflat baseline. We thus applied a sequential subtraction strategy³¹ to record the baseline using a two-blade chopper wheel that was synched with the laser at 5 Hz. The chopper wheel blocked the incoming laser beam from exciting the sample for every other shot. The absorbance change was calculated by sequentially dividing the baseline from the signal.

■ RESULTS AND DISCUSSION

We prepared three types of electrodes for charge recombination analysis. Pristine electrodes represent mesoporous TiO_2 film electrodes sensitized with bis(2,2'-bipyridine)(4,4'-diphosphonato-2,2'-bipyridine)-ruthenium bromide (RuP) without any additional treatment, the most commonly used photoanode in WS-DSPECs. When the pristine electrode undergoes a TiCl_4 -treatment as described in the Experimental Section, we obtain TiCl_4 -treated electrodes. Further depositing a thin layer of tantalum oxide over TiCl_4 -treated electrodes by ALD yields $\text{TiO}_2/\text{TaO}_x$ electrodes. With TiCl_4 -treatment and ALD, we did not observe significant changes in crystal structure and any change in TiO_2 particle size was too subtle to observe by scanning electron microscopy (SEM) (Figure S1). However, the sensitizer surface coverages estimated by

UV–vis absorption (Figure 1a) suggested a 13 and 33% decrease in surface area after TiCl_4 -treatment and ALD

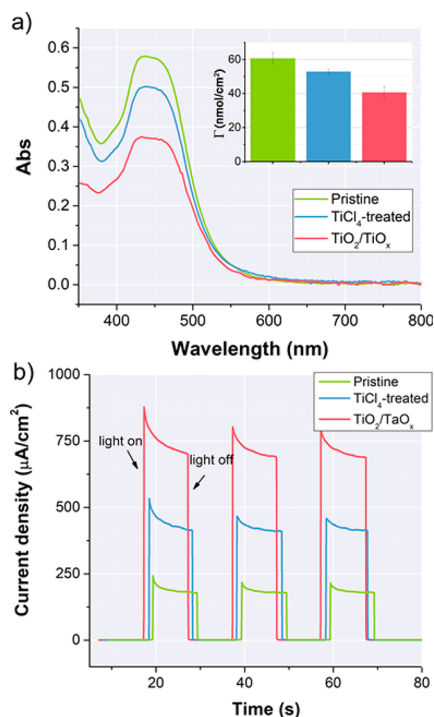


Figure 1. (a) UV–vis absorption spectra and surface coverages of sensitizers (Γ , inset) for the three types of electrodes under investigation. (b) Chronoamperometric measurement at an applied bias of 0.2 V. The measurement was conducted using hydroquinone (50 mM) as the electron donor under white light illumination (150 W xenon lamp, >410 nm, 100 mW/cm²).

coating, respectively. In the presence of hydroquinone as the electron donor, we measured the photocurrent–time profiles for the three types of electrodes (Figure 1b). Photocurrents from the TiCl_4 -treated and $\text{TiO}_2/\text{TaO}_x$ electrodes exhibited an increase by a factor of 2.3 and 3.9 relative to the pristine electrodes, respectively. This is consistent with previous reports that TiCl_4 -treatment and a core–shell structure can effectively improve the performance of dye-sensitized photoelectrodes.

Photoelectrochemical Impedance Spectroscopy. We used PEIS (photoelectrochemical impedance spectroscopy) to measure the ideality factor m in eq 4. PEIS experiments were carried out in galvanostatic mode at open-circuit under illumination. The electrode potential modulation in response to a sinusoidal current perturbation was recorded to construct Nyquist plots.

Typical Nyquist plots from PEIS are shown in Figure 2a. In the measured frequency range, the spectrum appeared as semicircles that shrank with increasing illumination intensity. We identify the frequency response as the electron transport and recombination processes in TiO_2 films and the data can be adequately fitted to a simple $R_s(R_pC)$ circuit (Figure 2a inset), where R_s , R_p , and C are the series resistance, and the resistance and capacitance from TiO_2 , respectively. The fitting results for the three types of electrodes are shown in Figure S2. The TiO_2 resistance in all cases decreased exponentially toward cathodic potential under illumination, which is expected as electrons populate more mobile states near the conduction band edge

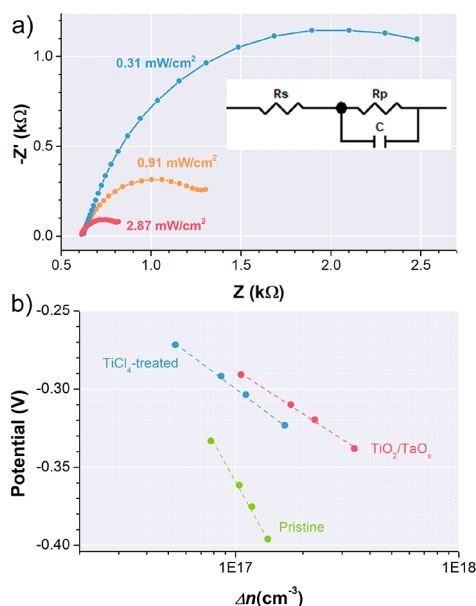


Figure 2. (a) PEIS Nyquist plots for a TiCl_4 -treated electrode at different illumination intensities. Inset: the equivalent circuit used for data fitting. (b) Semilog plot of the open-circuit potential as a function of the injected electron concentration. Dashed lines are linear fits using eq 6.

and traps states are filled. Without dye sensitization, the TiO_2 electrode showed a very large charge transfer resistance (a semicircle of large diameter), as plotted in Figure S3a. The TiO_2 capacitance, however, remained essentially unchanged for pristine electrodes, whereas it increased with more cathodic potentials for the TiCl_4 -treated and $\text{TiO}_2/\text{TaO}_x$ electrodes.

From the area under the capacitance–voltage curve (Figure S2b), the relationship between the open-circuit potential and electron concentration could be obtained and is plotted in Figure 2b. The integrated charge versus potential was then fitted to eq 6 to obtain values of the ideality factor m , and the results for the three types of electrodes are presented in Table 1. The integrated number of electrons for each electrode is referenced to the electron concentration at the most positive open-circuit potential (i.e., at the lowest illumination intensity). The ideality factor for TiCl_4 -treated and $\text{TiO}_2/\text{TaO}_x$ electrodes is between 1 and 2, close to the value commonly reported for DSSCs.^{27,28,32} The pristine electrode shows an m as high as 4.12, which is very likely an artifact. Since the capacitance of these electrodes was small and approximately constant with potential (Figure S2b), the integration to obtain charge as a function of potential is close to linear, instead of exponential as expected from eq 4. This suggests that the charging involves a high density of surface states for the pristine electrode and that only after TiCl_4 treatment does the dye-sensitized electrode/solution interface behave more like an ideal diode.

Intensity-Modulated Photovoltage Spectroscopy.

The fundamental equations governing IMVS are provided in the Supporting Information. Figure 3a shows typical Nyquist plots from IMVS measurement. Equation S7 suggests that the frequency response of the modulated term should appear in the first quadrant of a Nyquist plot (Figure 3a, I), in which the negative imaginary part is plotted against the real part of the voltage oscillation. The appearance of experimental data in the third quadrant (Figure 3a, III) is because an increase in the

Table 1. Fitting Results and Calculated Parameters

sample	$dV_{\text{light}}/d \log n$ (mV/dec)	m	$dV_{\text{light}}/d \log I_0$ (mV/dec)	$d \log k_{\text{IMVS}}/dV_{\text{light}}$ (dec/V)	α	β
pristine	-243.5 ± 11.8	4.12 ± 0.20	-84.5 ± 2.5	-10.79 ± 0.63	2.63 ± 0.20	0.25 ± 0.26
TiCl ₄ -treated	-105.0 ± 2.9	1.78 ± 0.05	-74.6 ± 0.4	-7.88 ± 0.42	0.83 ± 0.05	0.58 ± 0.06
TiO ₂ /TaO _x	-92.6 ± 3.3	1.57 ± 0.06	-77.5 ± 1.3	-6.98 ± 0.21	0.65 ± 0.03	0.55 ± 0.06

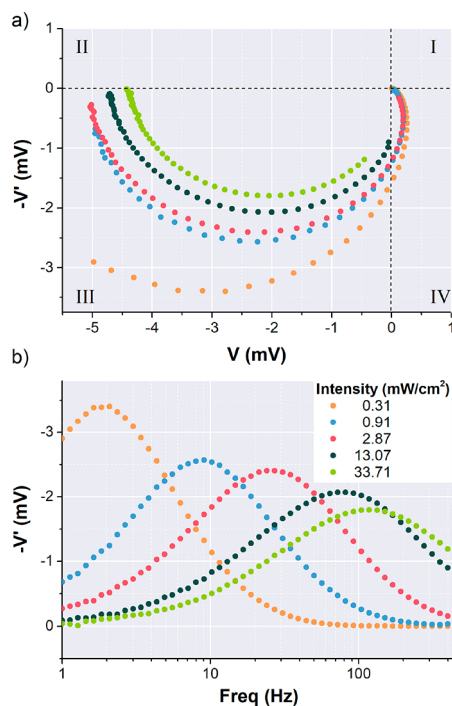


Figure 3. IMVS Nyquist (a) and Bode (b) plots for the pristine electrode at various illumination intensities. The four quadrants are indicated by Roman numerals.

electron population in TiO₂ induces a cathodic potential. In the Bode plot (Figure 3b), where the magnitude of the imaginary part is plotted against frequency, we can identify the recombination rate (k_{IMVS}) as the frequency (f_{IMVS}) at which the imaginary part reaches a maximum, as discussed in the Supporting Information:

$$k_{\text{IMVS}} = 2\pi f_{\text{IMVS}} \quad (14)$$

We measured the open-circuit potentials (V_{light}) of the three types of photoanodes as a function of light intensity that spans two orders of magnitude (Figure 4a). The corresponding recombination rates determined from IMVS data are plotted in Figure 4b. V_{light} is observed to shift cathodically with an exponential increase in light intensity, and k_{IMVS} scales exponentially with V_{light} . With m available from PEIS experiments and using eq 13 to fit Figure 4a, we can directly calculate α , and from Figure 4b, β can be deduced based on eq 11.

We obtained by this analysis fractional reaction orders for the three electrodes and their molecularity differs, as shown in Table 1. These fractional orders probably reflect the fact that recombination occurs via the multiple trap states that distribute exponentially in energy in TiO₂. The results also showed that recombination in the pristine electrode was close to a unimolecular process with fractional reaction order as large as 2.63 with respect to the oxidized sensitizer concentration (β is close to 0 considering fitting errors). The high reaction order, although it may be an indication of

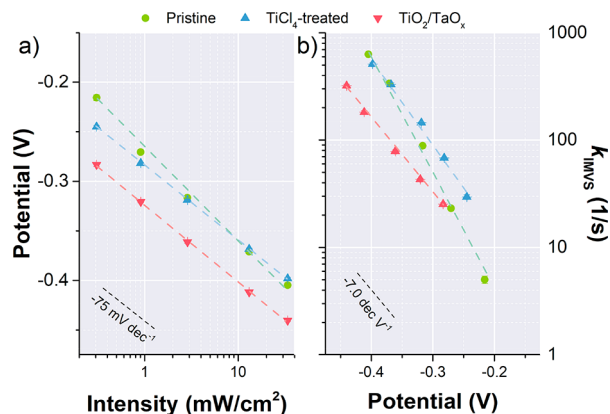


Figure 4. (a) Open-circuit potentials of the photoelectrodes under illumination at different intensities. (b) Recombination rates determined from IMVS at different open-circuit potentials under illumination. Dashed lines are linear fitting results.

abundant trap states in pristine electrodes, can also result from the application of an inappropriate model. As noted above, the charging of pristine electrodes does not follow the diode equation; therefore, eq 4 cannot be used with pristine electrodes for recombination analysis. For TiCl₄-treated and core-shell electrodes, IMVS measurements suggested a bimolecular recombination process with fractional orders with respect to both oxidized sensitizer molecules and electrons, indicating that the removal of trap states by TiCl₄ treatment altered the recombination mechanism. Moreover, we observed a very similar dependence of V_{light} on the illumination intensity for TiCl₄-treated and TiO₂/TaO_x electrodes. This is reflected in Figure 4a as two parallel lines offset by about 40 mV in potential at the same light intensity. If we assume the same V_{dark} , A , n_d , and $\frac{m}{\alpha + \beta}$ for the TiCl₄-treated and TiO₂/TaO_x electrodes, then their potential offset at the same illumination intensity can be expressed as follows based on eq 10:

$$\Delta V = V_2 - V_1 = -\frac{2.3mkT}{q(\alpha + \beta)} \log \frac{k_{r1}}{k_{r2}} \quad (15)$$

where the subscripts 1 and 2 represent TiCl₄-treated and TiO₂/TaO_x electrodes, respectively. Using a ΔV of -40 mV and a slope of -76 mV/dec ($-\frac{2.3mkT}{q(\alpha + \beta)}$), the average of slopes in Figure 4a for the two electrodes, we calculated that the recombination rate coefficient (k_{r1}) for TiCl₄-treated electrodes is about 3.4 times larger than that of the TiO₂/TaO_x electrodes (k_{r2}), indicating that the core-shell structure indeed slows down charge recombination in the dye-sensitized photoelectrode. According to eq 12, at the same V_{light} the recombination rate measured from IMVS is proportional to k_r ; thus, we can estimate k_{r1} to be 4.1–3.1 times larger than k_{r2} from Figure 4b, which agrees well with the value calculated from the potential–light intensity profile.

The fractional reaction orders we report here are in disagreement with the conclusions from earlier studies (mainly by time-resolved absorption spectroscopy) that eq 1 is a bimolecular process with unity reaction order with respect to both sensitizer and electron concentrations ($\alpha = \beta = 1$).^{8–10} We believe that this discrepancy stems from different measurement conditions, as will be discussed in detail below.

In PEIS measurement, we can also define an electron recombination rate (k_{EIS}) as the inverse of $R_{\text{p}}C$. k_{EIS} for a TiCl_4 -treated electrode was measured at different open-circuit potentials (by tuning the illumination intensity) and compared with k_{IMVS} measured under the same conditions (Figure 5).

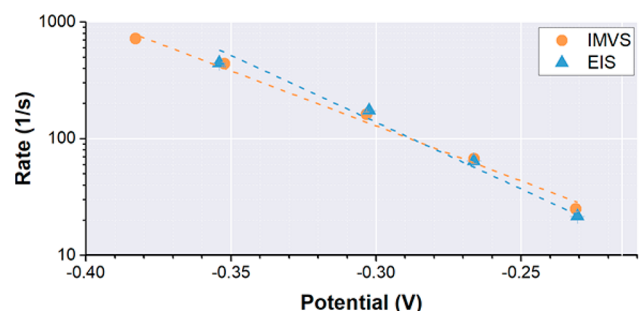


Figure 5. Comparison of recombination rates measured by IMVS and PEIS for a TiCl_4 -treated electrode.

Interestingly, k_{EIS} and k_{IMVS} are in close agreement. This suggests that the recombination process probed by IMVS is actually the discharging of the injected electrons into the TiO_2 film, which is limited by the TiO_2 electrode resistance and capacitance. The fact that the RC time constant plays a role in charge recombination is also reported by Lin et al. in their study of carrier lifetimes in nanocrystal-based solar cells.³³

The fact that PEIS and IMVS characterize the same recombination process suggests that a similar kinetic analysis, as shown in Figure 4, may also be applied to the PEIS data. PEIS also provides insight into the slower recombination rate measured by IMVS in the core–shell structure. As shown in Figure S2, both the TiO_2 resistance and capacitance are increased by TaO_x coating, leading to a longer RC time constant. However, we found that IMVS measurements were advantageous over PEIS under intense illumination, where the injected electrons raise the potential close to the flat-band potential of TiO_2 , because the semicircle in the PEIS Nyquist plot shrinks with increasing light intensity, and the equivalent circuit cannot accurately fit the deformed spectra at high illumination intensity (Figure S3b).

It is worth noting that k_{IMVS} is used as a first-order rate constant throughout the analysis, even though the actual reaction order for electrons is fractional. As in Figure S4, the characteristic time constant from IMVS (the frequency at the apex point in the Bode plot) for $\beta < 1$ is much smaller than the actual electron recombination rate k_1 . When $k_1 = 100 \text{ s}^{-1}$, k_{IMVS} for $\beta = 1$ and $\beta = 0.8$ are 100 and 0.045 s^{-1} , respectively. Therefore, if we measure a k_{IMVS} of 100 s^{-1} for TiCl_4 -treated electrodes and use $\beta = 0.58$ in eq S2, then the actual k_1 would be larger than 100 s^{-1} by several orders of magnitude, which contradicts the time scale measured by PEIS. The closely related recombination rates from PEIS and IMVS (Figure 5) also support the apparent reaction order of 1, because voltage decay in a RC circuit follows first-order kinetics. Direct observation of first-order decay profiles in TPVD (transient

photovoltage decay) experiments³⁴ also supports the idea that electron recombination is a first-order process; thus, k_{IMVS} can be approximated as a first-order rate constant with small perturbation techniques (IMVS, PEIS, and TPVD) in which potential (or voltage) decay is treated as linear with electron concentration instead of being exponential as in eq 4. The fractional orders we obtained using eqs 11 and 13 are from Figure 4, in which open-circuit potentials and recombination rates were measured by varying light intensity across 2 orders of magnitude. Although the individual data points in Figure 4, when measured by IMVS, can be treated as first-order rate constants, they collectively revealed the fractional orders over wide range of light intensities.

Transient Absorption Spectroscopy. In the ideal case in which one electron recombines with one oxidized sensitizer molecule simultaneously, one would expect the same lifetime for both electrons and oxidized sensitizers. Therefore, we also characterized the three types of photoanodes through the bleaching recovery dynamics of RuP upon excitation. With the photoelectrodes held in galvanostatic mode (i.e., under open-circuit conditions), we conducted these transient absorbance experiments at various probe light intensities, since the IMVS data suggested an intensity dependence of the recombination rate. Figure 6a (raw data plotted in Figure S5) shows the

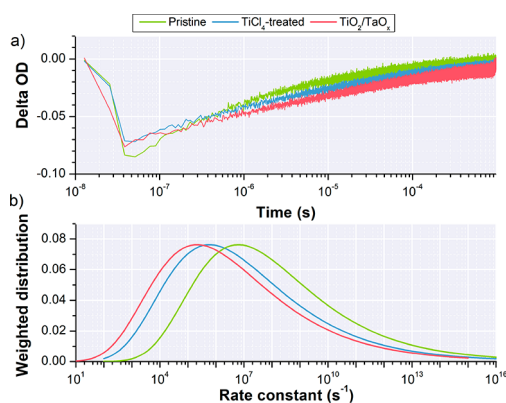


Figure 6. (a) Bleaching recovery kinetics and (b) the corresponding rate constant distribution at 470 nm for the three types of electrode at a probe light intensity of 11.64 mW/cm^2 .

sensitizer bleaching recovery kinetics at 470 nm within 1 ms after laser excitation. Note that there is an instrumental rise time of about 30 ns in the TA system.

The bleaching recovery data show multiphasic recombination kinetics as commonly reported in the literature for DSPECs. We fitted the bleaching recovery kinetics to the Kolrausch–Williams–Watts (KWW) stretched exponential function:

$$\Delta A = A_1 \exp \left[- \left(\frac{t}{\tau_{\text{KWW}}} \right)^{\beta_{\text{KWW}}} \right] + A_2 \quad (16)$$

where ΔA is the absorbance change over time t ; A_1 and A_2 are constant; τ_{KWW} is the characteristic time constant; and β_{KWW} is between 0 and 1, a parameter describing the distribution width of the first-order processes. The KWW kinetic model has been widely applied to describe the complex charge transfer kinetics at the dye–semiconductor interfaces.^{35–39} The inverse Laplace transform of eq 16 presents the distribution of the underlying

rate constants, and the distribution function G_{KWW} is shown below:⁴⁰

$$G_{\text{KWW}}(1/\tau) = -\frac{\tau\tau_{\text{KWW}}}{\pi\tau^2} \sum_{k=0}^{\infty} \frac{(-1)^k}{k!} \sin(\pi\beta_{\text{KWW}}k) \Gamma(k\beta_{\text{KWW}} + 1) \left(\frac{\tau}{\tau_{\text{KWW}}}\right)^{k\beta_{\text{KWW}}+1} \quad (17)$$

We fixed β_{KWW} at 0.2, and the fitted curves, τ_{KWW} and the $\text{adj-}R^2$, are shown in Figure S5. The data collected at low probe light intensities are not included for further analysis due to low $\text{adj-}R^2$ (<0.9), and the rest are fed into eq 17 for rate distribution analysis. As shown in Figure 6b, the rate constants for all electrodes distribute over more than 6 orders of magnitude, implying highly dispersive recombination processes. The most probable rate constant in the pristine electrode is about 10^7 s^{-1} , and the corresponding rates for TiCl_4 -treated and $\text{TiO}_2/\text{TaO}_x$ electrodes are lower by about 1 and 1.5 orders of magnitude, respectively. For the same electrode, the rate distribution did not show a strong correlation with the probe light intensity except for the $\text{TiO}_2/\text{TaO}_x$ electrode, where the rate distribution shifted slightly toward faster recombination with higher probe light intensity.

We observed that in all cases the most probable rate constants given by TA are larger than k_{IMVS} by 3 orders of magnitude even though the probe light intensities in TA were comparable to those in IMVS. This large discrepancy was noted before when we characterized the recombination process of dye-sensitized photoanodes using TPVD, and we have previously ascribed it to the different electrolytes used in the experiments.³⁴ With the same electrolyte, the same effect appeared here, and this prompts us to reconcile the different lifetimes obtained by different techniques.

Although both IMVS and TA apply light perturbation to dye-sensitized photoanodes, there is a pronounced difference in the perturbation amplitude of the two techniques. The light perturbation used in IMVS is set at 10% of the steady-state illumination intensity, and the perturbation at the highest illumination intensity we used is about 3 mW/cm^2 at 470 nm. In the case of TA, a Nd:YAG laser pulsed 6.5 mJ at 532 nm in 10 ns, which, with a laser spot of 0.7 cm^2 , translates to a light intensity as high as 10^9 mW/cm^2 . The high-intensity laser excitation is expected to excite more electrons into TiO_2 . The initial bleaching amplitude in Figure S5 was close to 0.1, corresponding to an excited RuP concentration of 10^{19} cm^{-3} . (See the Supporting Information for calculation details.) From Figure 2b, an electron concentration of 10^{19} cm^{-3} will induce an open-circuit potential much more cathodic than those measured in PEIS and IMVS (as well as those measured under solar illumination), although this transient potential change may be hard to record due to the electrode RC rise time. In contrast, the injected electron concentration estimated from PEIS is around 10^{17} cm^{-3} . With 100 times more electrons injected, one would expect an accelerated recombination from TA. A stronger perturbation beam than the probe beam in TA can also explain the weak dependence of the recombination rate on probe light intensity. Our observation that TA measurements report a faster recombination process than IMVS because of higher injected electron concentrations is in line with the early report from Haque et al.¹¹ They report a strong dependence of the recombination kinetics on laser

excitation intensity, and this is explained by the occupancy of conduction band/trap states: the more of those states occupied by electrons, the faster the recombination. They also note that the charge recombination cannot be simply modeled with Marcus electron transfer theory, because a more negative bias and a negative shift of the trap states/conduction band energy result in opposite effects on the charge recombination: the former (latter) accelerates (retards) the process.

Therefore, previous TA reports of $\alpha = \beta = 1$ in eq 1 may be understood as recombination from high electron occupancy conditions, which, however, are not accessible from typical solar illumination. Lowering the laser energy so that the number of laser-induced injected electrons is close to those in IMVS may allow observation of bleaching recovery rate comparable to k_{IMVS} , but this may also bring challenges in acquiring data with good signal-to-noise ratio.

CONCLUSIONS

We have explored the charge recombination processes in three types of dye-sensitized photoelectrodes through a combination of techniques based on electrochemistry, photoelectrochemistry, and transient spectroscopy. When recombination kinetics are measured by TA, they are fast because of the high transient concentration of electrons and oxidized sensitizer molecules, and the process is governed by a distributed rate law. This is consistent with previous conclusions of Haque et al.¹¹ However, the rate equation and average lifetime are not very relevant to the operation of the photoelectrochemical cell (under DC conditions at one sun) because of the high laser fluence.

In PEIS or IMVS measurements, the light intensity is closer to that used in WS-DSPECs, and the sinusoidal perturbation of electron concentration is small relative to the steady-state light intensity. Under these conditions one measures slower charge recombination by three orders of magnitude, consistent with earlier photovoltage decay measurements. Dye-sensitized electrodes in which TiO_2 surface states are passivated by TiCl_4 treatment or by a Ta_2O_5 shell follow the diode equation with ideality factors in the range of 1.6–1.8. However, analysis of the data at any single illumination intensity gives kinetics that are dominated by the RC time constant of the electrode/solution interface, a fact that has not previously been appreciated. The RC time constant explains the apparent first-order decay that has been observed in transient photovoltage measurements. Although both TA and IMVS measurements can associate the semiconductor surface properties (such as TiCl_4 -treatment and core/shell structure) with a recombination lifetime, we show by using IMVS rate analysis that the changes in the steady-state open-circuit potential when the light intensity is varied reveal that charge recombination follows a bimolecular rate law with fractional reaction orders.

This study underscores the utility of IMVS as a complementary technique to TA and PEIS for exploring the recombination dynamics of dye-sensitized photoelectrodes in aqueous media used in water splitting cells. The kinetic analysis described here gives the recombination rate law that is most relevant to DC operation of the photoelectrochemical cell, and it should be possible to extend this analysis to better understand the recombination processes in full WS-DSPECs in which nanoparticle and molecular catalysts are involved in water oxidation.

■ ASSOCIATED CONTENT**Supporting Information**

The Supporting Information is available free of charge on the ACS Publications website at DOI: 10.1021/jacs.8b04878.

XRD and SEM images for electrodes undergoing different surface treatments, resistance and capacitance data from PEIS measurements, derivation of IMVS principles, TA data analysis (PDF)

■ AUTHOR INFORMATION**Corresponding Author**

*tem5@psu.edu

ORCID

Pengtao Xu: 0000-0002-4470-446X

Thomas E. Mallouk: 0000-0003-4599-4208

Notes

The authors declare no competing financial interest.

■ ACKNOWLEDGMENTS

We thank Zhifei Yan and Liqiang Ren for helpful discussions in the preparation of the manuscript. This work was supported by the Office of Basic Energy Sciences, Division of Chemical Sciences, Geosciences, and Energy Biosciences, Department of Energy, under contract DE-FG02-07ER15911.

■ REFERENCES

- (1) Brennaman, M. K.; Dillon, R. J.; Alibabaei, L.; Gish, M. K.; Dares, C. J.; Ashford, D. L.; House, R. L.; Meyer, G. J.; Papanikolas, J. M.; Meyer, T. J. *J. Am. Chem. Soc.* **2016**, *138*, 13085–13102.
- (2) Xu, P.; McCool, N. S.; Mallouk, T. E. *Nano Today* **2017**, *14*, 42–58.
- (3) Li, F.; Yang, H.; Li, W.; Sun, L. *Joule* **2018**, *2*, 36–60.
- (4) Youngblood, J. W.; Lee, S. H. A.; Kobayashi, Y.; Hernandez-Pagan, E. A.; Hoertz, P. G.; Moore, T. A.; Moore, A. L.; Gust, D.; Mallouk, T. E. *J. Am. Chem. Soc.* **2009**, *131*, 926–927.
- (5) Chen, H.-Y.; Ardo, S. *Nat. Chem.* **2017**, *10*, 17–23.
- (6) Jiang, J.; Spies, J. A.; Swierk, J. R.; Matula, A. J.; Regan, K. P.; Romano, N.; Brennan, B. J.; Crabtree, R. H.; Batista, V. S.; Schmuttenmaer, C. A.; Brudvig, G. W. *J. Phys. Chem. C* **2018**, *122*, 13529–13539.
- (7) Brennan, B. J.; Regan, K. P.; Durrell, A. C.; Schmuttenmaer, C. A.; Brudvig, G. W. *ACS Energy Lett.* **2017**, *2*, 168–173.
- (8) Thompson, D. W.; Kelly, C. A.; Farzad, F.; Meyer, G. J. *Langmuir* **1999**, *15*, 650–653.
- (9) Kilså, K.; Mayo, E. I.; Kuciauskas, D.; Villahermosa, R.; Lewis, N. S.; Winkler, J. R.; Gray, H. B. *J. Phys. Chem. A* **2003**, *107*, 3379–3383.
- (10) Kelly, C. A.; Farzad, F.; Thompson, D. W.; Stipkala, J. M.; Meyer, G. J. *Langmuir* **1999**, *15*, 7047–7054.
- (11) Haque, S. A.; Tachibana, Y.; Willis, R. L.; Moser, J. E.; Grätzel, M.; Klug, D. R.; Durrant, J. R. *J. Phys. Chem. B* **2000**, *104*, 538–547.
- (12) Brigham, E. C.; Meyer, G. J. *J. Phys. Chem. C* **2014**, *118*, 7886–7893.
- (13) Ponomarev, E. A.; Peter, L. M. *J. Electroanal. Chem.* **1995**, *396*, 219–226.
- (14) Schlichthörl, G.; Huang, S. Y.; Sprague, J.; Frank, A. J. *J. Phys. Chem. B* **1997**, *101*, 8141–8155.
- (15) Krüger, J.; Plass, R.; Grätzel, M.; Cameron, P. J.; Peter, L. M. *J. Phys. Chem. B* **2003**, *107*, 7536–7539.
- (16) Pockett, A.; Eperon, G. E.; Peltola, T.; Snaith, H. J.; Walker, A.; Peter, L. M.; Cameron, P. J. *J. Phys. Chem. C* **2015**, *119*, 3456–3465.
- (17) Thorne, J. E.; Jang, J.-W.; Liu, E. Y.; Wang, D. *Chem. Sci.* **2016**, *7*, 3347–3354.
- (18) Hagfeldt, A.; Boschloo, G.; Sun, L.; Kloo, L.; Pettersson, H. *Chem. Rev.* **2010**, *110*, 6595–6663.

- (19) O'Regan, B. C.; Durrant, J. R.; Sommeling, P. M.; Bakker, N. J. *J. Phys. Chem. C* **2007**, *111*, 14001–14010.
- (20) Murakami, T. N.; Miyadera, T.; Funaki, T.; Cojocaru, L.; Kazaoui, S.; Chikamatsu, M.; Segawa, H. *ACS Appl. Mater. Interfaces* **2017**, *9*, 36708–36714.
- (21) Choe, G.; Kang, J.; Ryu, I.; Song, S. W.; Kim, H. M.; Yim, S. *Sol. Energy* **2017**, *155*, 1148–1156.
- (22) Adli, H. K.; Harada, T.; Nakanishi, S.; Ikeda, S. *Phys. Chem. Chem. Phys.* **2017**, *19*, 26898–26905.
- (23) Knauf, R. R.; Kalanyan, B.; Parsons, G. N.; Dempsey, J. L. *J. Phys. Chem. C* **2015**, *119*, 28353–28360.
- (24) Sherman, B. D.; Ashford, D. L.; Lapedes, A. M.; Sheridan, M. V.; Wee, K.-R.; Meyer, T. J. *J. Phys. Chem. Lett.* **2015**, *6*, 3213–3217.
- (25) Gish, M. K.; Lapedes, A. M.; Brennaman, M. K.; Templeton, J. L.; Meyer, T. J.; Papanikolas, J. M. *J. Phys. Chem. Lett.* **2016**, *7*, 5297–5301.
- (26) Huang, S. Y.; Schlichthörl, G.; Nozik, A. J.; Grätzel, M.; Frank, A. J. *J. Phys. Chem. B* **1997**, *101*, 2576–2582.
- (27) Ocakoglu, K.; Yakuphanoglu, F.; Durrant, J. R.; Icli, S. *Sol. Energy Mater. Sol. Cells* **2008**, *92*, 1047–1053.
- (28) Barnes, P. R. F.; Anderson, A. Y.; Durrant, J. R.; O'Regan, B. C. *Phys. Chem. Chem. Phys.* **2011**, *13*, 5798–5816.
- (29) McCool, N. S.; Swierk, J. R.; Nemes, C. T.; Saunders, T. P.; Schmuttenmaer, C. A.; Mallouk, T. E. *ACS Appl. Mater. Interfaces* **2016**, *8*, 16727–16735.
- (30) Gillaizeau-Gauthier, I.; Odobel, F.; Alebbi, M.; Argazzi, R.; Costa, E.; Bignozzi, C. A.; Qu, P.; Meyer, G. J. *Inorg. Chem.* **2001**, *40*, 6073–6079.
- (31) Rimshaw, A.; Grieco, C.; Asbury, J. B. *Rev. Sci. Instrum.* **2015**, *86*, 066107.
- (32) Barr, T. J.; Meyer, G. J. *ACS Energy Lett.* **2017**, *2*, 2335–2340.
- (33) Lin, W. M. M.; Bozyigit, D.; Yarema, O.; Wood, V. J. *Phys. Chem. C* **2016**, *120*, 12900–12908.
- (34) Swierk, J. R.; McCool, N. S.; Mallouk, T. E. *J. Phys. Chem. C* **2015**, *119*, 13858–13867.
- (35) Abrahamsson, M.; Johansson, P. G.; Ardo, S.; Kopecky, A.; Galoppini, E.; Meyer, G. J. *J. Phys. Chem. Lett.* **2010**, *1*, 1725–1728.
- (36) Hu, K.; Blair, A. D.; Piechota, E. J.; Schauer, P. A.; Sampaio, R. N.; Parlani, F. G. L.; Meyer, G. J.; Berlinguette, C. P. *Nat. Chem.* **2016**, *8*, 853–859.
- (37) Farnum, B. H.; Wee, K.-R.; Meyer, T. *Nat. Chem.* **2016**, *8*, 845–852.
- (38) DiMarco, B. N.; Troian-Gautier, L.; Sampaio, R. N.; Meyer, G. J. *Chem. Sci.* **2018**, *9*, 940–949.
- (39) Troian-Gautier, L.; DiMarco, B. N.; Sampaio, R. N.; Marquard, S. L.; Meyer, G. J. *J. Am. Chem. Soc.* **2018**, *140*, 3019–3029.
- (40) Lindsey, C. P.; Patterson, G. D. *J. Chem. Phys.* **1980**, *73*, 3348–3357.